Journal of Controlled Release xxx (2014) xxx–xxx

Contents lists available at ScienceDirect

Journal of Controlled Release

journal homepage: www.elsevier.com/locate/jconrel

Real time Raman imaging to understand dissolution performance of amorphous solid dispersions

Francesco Tres [a], Kevin Treacher [b], Jonathan Booth [b], Les P. Hughes [b], Stephen A.C. Wren [b], Jonathan W. Aylott [a], Jonathan C. Burley [a,*]

[a] School of Pharmacy, Boots Science Building, University of Nottingham, Nottingham NG7 2RD, United Kingdom
[b] Pharmaceutical Development, AstraZeneca, Macclesfield, SK10 2NA, United Kingdom

ARTICLE INFO

Article history:
Received 28 March 2014
Accepted 30 May 2014
Available online xxxx

Keywords:
Poorly soluble drugs
Amorphous solid dispersions
Solid-state transformations
Raman imaging
Intrinsic dissolution rate
Multi-variate curve resolution (MCR)

ABSTRACT

We have employed for the first time Raman spectroscopic imaging along with multi-variate curve resolution (MCR) analysis to investigate in real time and *in-situ* the dissolution mechanisms that underpin amorphous solid dispersions, with data being collected directly from the dosage form itself. We have also employed a novel rotating disk dissolution rate (RDDR) methodology to track, through the use of high-performance liquid chromatography (HPLC), the dissolution trends of both drug and polymer simultaneously in multi-component systems. Two formulations of poorly water-soluble felodipine in a polymeric matrix of copovidone VA64 which have different drug loadings of 5% and 50% w/w were used as models with the aim of studying the effects of increasing the amount of active ingredient on the dissolution performance. It was found that felodipine and copovidone in the 5% dispersion dissolve with the same dissolution rate and that no Raman spectral changes accompanied the dissolution, indicating that the two components dissolve as single entity, whose behaviour is dominated by water-soluble copovidone. For the 50% drug-loaded dispersion, partial RDDR values of both felodipine and copovidone were found to be extremely low. MCR Raman maps along with classical Raman/X-ray powder diffraction (XRPD) characterisation revealed that after an initial loss of copovidone from the extrudate the drug re-crystallises, pointing to a release dynamics dependent on the low water solubility and high hydrophobicity of felodipine. Raman imaging revealed different rates of transition from amorphous to crystalline felodipine at different locations within the dosage form.

1. Introduction

A high number of new chemical entities emerging from the drug development process show pharmacological activity, but at the same time are characterised by poor dissolution and solubility profiles [1]. As a result, there is a strong push to develop innovative formulations for the delivery of such compounds so that the desired oral bioavailability and pharmacological effects are achieved. An increasingly popular class of formulation is represented by amorphous solid dispersions, which are prepared by co-processing the drug and a water-soluble or water-swellable polymeric carrier, commonly *via* spray drying or hot melt extrusion [2,3]. The resultant dispersion, as widely demonstrated for several poorly soluble compounds, has an improved dissolution profile and consequently bioavailability compared to the pure drug [4]. This is attributed to the fact that the drug within the dispersion exists in the amorphous form, which gives a higher dissolution rate than the corresponding crystalline form, and also due to the presence of the water-soluble polymer [5,6].

One of the key challenges for deploying amorphous solid dispersions in real-world formulations is the understanding of the dissolution performance. Although this is very relevant, due to the fact that the dissolution performance limits the *in vivo* efficacy, relatively few studies have been conducted to investigate the dissolution mechanisms that underpin these systems. As reported by Craig, [7] the dissolution mechanism of amorphous solid dispersions is characterised by a number of critical processes, which primarily depend on the chemical nature of the components and on the drug-to-polymer ratio. In relation to these parameters, Craig classified the drug release from amorphous solid dispersions as polymer-controlled or drug-controlled. It has been demonstrated that the re-crystallisation of the drug either in the solid state or after precipitation in solution, [8,9] the formation of nano- and micro-particles during the dissolution [10] and also the behaviour of the polymer itself, [11] strongly contribute to the final dissolution performance. Amorphous solid dispersion dissolution mechanisms are extremely difficult to de-convolute due to several processes occurring simultaneously.

* Corresponding author.
E-mail address: jonathan.burley@nottingham.ac.uk (J.C. Burley).

http://dx.doi.org/10.1016/j.jconrel.2014.05.061
0168-3659/

Classical methods of investigating drug release such as the use of USP dissolution apparatuses [12] do not offer any chemical or spatially-resolved information on potential changes of the solid form (*e.g.* from amorphous to crystalline, polymorphic transformations or formation of hydrate states) during the dissolution, since the data are collected from the solution, rather than directly from the solid dosage form itself. Given the limitations of the conventional dissolution apparatuses, innovative methods have been developed in an attempt to provide a more complete picture of the drug release. Such methods have included mid-IR, [13,14] near-IR [15,16] and magnetic resonance imaging (MRI) [8,17]. Mid-IR and near-IR provide chemical information, but also have a significant drawback; they are very sensitive to water which clearly limits the use of these techniques in aqueous environments. MRI is attractive as it can offer three-dimensional information, however it provides little chemical specificity.

Raman spectroscopy, theoretically, offers advantages/complementarities compared to these techniques. It provides chemically detailed and two-dimensional spatial information ('hyper-spectral data', one spectrum per pixel) and is able to readily differentiate between amorphous and crystalline solid forms [18,19]. These properties are significant since the chemical and physical forms of the drug can change during the course of the dissolution test [8,9,14]. Moreover, with respect to mid-IR and near-IR, Raman spectroscopy is relatively insensitive to water [20]. Raman spectroscopy is therefore an appropriate technique to investigate how the solid state properties of the drug affect its release and for this reason was employed in this work to understand the performance of amorphous solid dispersions during dissolution in aqueous media.

An amorphous solid dispersion of felodipine, the active ingredient, in a polymeric matrix of copovidone VA64, was used as model formulation. Felodipine is an antihypertensive drug, characterised by high permeability and low water solubility (lower than 0.5 mg/lt) [21]. Copovidone VA64 is a highly water-soluble polymer (solubility higher than 100 mg/lt), [22] recognised as a chemical analogue of polyvinylpyrrolidone (PVP). In previous studies, PVP and copovidone VA64 have been successfully used to prepare one-phase amorphous felodipine binary mixtures over a range of composition (0–70% drug loading), showing the ability to inhibit re-crystallisation and to increase the dissolution rate of poorly soluble felodipine [23–27]. The physical mixture of crystalline felodipine and copovidone VA64 has been shown instead to have a small increase in dissolution rate when compared to pure crystalline felodipine, further demonstrating how the physical state of the active ingredient (*e.g.* amorphous *vs.* crystalline) affects the whole dissolution performance regardless the presence or absence of the polymer in the formulation [8]. This work follows on from the recent paper by Langham et al., where the use of a combined spectrophotometric and magnetic resonance imaging technique to investigate the dissolution mechanisms of felodipine–copovidone spray-dried amorphous solid dispersions was described [8]. It was found that the dissolution behaviour of the high drug-loaded amorphous solid dispersions is governed by the low aqueous solubility of felodipine and by the re-crystallisation (confirmed by off-line XRPD) of the drug.

In the present work, we investigated formulations which have different drug loadings (5% and 50% w/w), with the aim of studying the effects of increasing the amount of active ingredient on the dissolution performance. Two different approaches were employed to probe the dissolution performance of amorphous solid dispersions. The first used Raman spectroscopy and the second uses a rotating disk dissolution rate (RDDR) test. Our RDDR method, with respect to conventional intrinsic dissolution rate (IDR) test described in the USP and in the European Pharmacopoeia, [12,28] employs HPLC to separate the drug from the polymer and ultimately allows us to measure the performance in aqueous media of multi-component systems.

The aim of this work is to investigate whether Raman spectroscopy provides additional chemical and spatial information regarding the dissolution mechanisms that underpin amorphous solid dispersions, used in conjunction with RDDR dissolution test.

2. Materials and methods

2.1. Preparation of amorphous felodipine and extrudate solid dispersions

The amorphous form of felodipine was obtained by heating the drug as received (AstraZeneca, Macclesfield, United Kingdom) in the oven to 160 °C and, after melting, cooling back to room temperature. Visual inspection and Raman spectroscopy confirmed the formation of the amorphous form and the absence of crystalline material within the detection limits (*ca.* 0.5% or better). 5% and 50% drug-loaded amorphous solid dispersions of felodipine in copovidone (BASF, Ludwigshafen, Germany) were prepared using a co-rotating twin-screw extruder (Thermo Scientific HAAKE MiniLab II). Felodipine and copovidone were pre-mixed for 20 min in a Turbula T2F mixer (Willy A. Bachofen AG Mashinefabrik). The extruder was manually fed with the physical mixture. The screw speed was set to 150 rpm and the temperature to 160 °C. The extrudates with spaghetti shape were then collected, cooled to room temperature and manually milled to fine powder. X-ray powder diffraction confirmed the formation of the amorphous solid dispersion and the absence of crystalline material (Figure S1).

2.2. X-ray powder diffraction (XRPD)

XRPD patterns were obtained using a PANalytical CubiX PRO diffractometer. Samples were exposed to Cu-Kα radiation at a voltage of 45 kV and a current of 40 mA. After being smeared onto the holder, samples were scanned from 2° to 40° 2θ, with a step size of 0.02° 2θ.

2.3. Rotating disk dissolution rate (RDDR)

RDDR testing was carried on using the rotating disk system, also known as 'Woods apparatus'. The die cavity has a diameter of 8 mm with subsequent exposed sample surface area of 0.5 cm^2. About 250 mg of extrudate powder was compressed under a compression force of 2000 kg using a manual IR press (Specac). The experiment was performed in a Sotax AT7 semi-automated dissolution bath equipped with an automated sample collector. Compressed discs were immersed in 500 ml of deionised water at 37 °C (±0.5), at 100 rpm rotational speed. The automated sample collector removed aliquots of sample from the dissolution medium at regular time intervals over 120 min. The samples were then analysed by reverse phase high performance liquid chromatography (RP-HPLC). Both the experiments for 5 and 50% extrudates were performed in triplicate. HPLC analysis was carried out using a Agilent 1100 with UV detection at 210 nm, equipped with an Agilent PLRP-S 300 Å 3 μm 50 mm column (polystyrene/divinylbenzene stationary phase). The flow rate was set to 1.0 ml/min and the temperature of the column was kept at 40 °C. A linear gradient elution was used starting at 40% acetonitrile/60% deionised water and ending at 90% acetonitrile/10% deionised water after 3.5 min, with chromatograms collected up to 5 min. A series of standard solutions of felodipine and copovidone were prepared to generate a calibration curve covering the concentration range of dissolved sample. The partial RDDR of both drug and polymer was calculated using linear regression analysis [12,28]. The partial RDDR of the substance tested was determined from the slope of the regression line.

2.4. Raman spectroscopy

We investigated the dissolution performance of compressed extrudate powder. Spherical compacts with a diameter of 5 mm and a weight of 50 mg were prepared with a manual IR press (Specac) using a compression force of *ca.* 20 kN. The dissolution test was performed in a flow cell, which is illustrated in Figure S2. Deionised water was

Please cite this article as: F. Tres, et al., Real time Raman imaging to understand dissolution performance of amorphous solid dispersions, J. Control. Release (2014), http://dx.doi.org/10.1016/j.jconrel.2014.05.061

used as dissolution medium and the flow rate was set to 10 ml/min. The flow cell was placed under the objective of the Raman microscope and data were collected as function of time using a Horiba LabRAM HR confocal microscope/spectrometer. The system has an automated xyz stage (Märzhäuser) for mapping. In all the experiments, a near-IR laser (785 nm) of 250 mW power was employed. Spectra were acquired using a 50 × objective and a 300 μm confocal hole. A 600 lines/mm rotatable diffraction grating along a path length of 800 mm was used to simultaneously scan a range of frequencies. Raman spectra were collected using a SYNAPSE CCD detector (1024 pixels). During the dissolution experiment, before each map being acquired, the z-axis position of the sample was adjusted to maximise the Raman signal. For both formulations (5% and 50% felodipine), spectra were obtained mapping an area of 500 × 500 μm with a grid spacing of 50 μm along both x-axis and y-axis, a total of 121 spectra for map. As each individual spectrum was collected for 1 s, repeated once in order to automatically remove the cosmic rays, the whole map required only 5 min. For the 5% extrudate compact, eight maps were acquired across a 70 minute time frame in the spectral range from 1100 to 1750 cm^{-1} (finger print region). For the 50% extrudate compact, eight maps were acquired over 1705 min (28 h25) in the phonon-mode (30–400 cm^{-1}) and finger print (1100–1750 cm^{-1}) regions using a fixed grating to allow relatively rapid mapping. In the latter case, the phonon-mode range was also scanned because it is extremely sensitive to the different solid forms (amorphous, crystalline, *etc.*) and therefore the potential drug re-crystallisation can be readily detected [18,19]. All the spectra from each map were integrated to produce a single averaged spectrum corresponding to each time point. In this way, it was possible to determine any spectral changes occurring during the dissolution test.

To obtain spatially-resolved information from the 50% extrudate compact, the dissolution experiment was repeated increasing significantly the spatial resolution. Seven maps were acquired over 1705 min (28 h25) in the spectral range between 1100 and 1750 cm^{-1}, across a 500 × 1000 μm area at a grid spacing of 15 μm along the x-axis, and 30 μm along the y-axis, a total of 1156 spectra per map. As the data acquisition time was 2 s for each spectrum, repeated once, each map required 1 h and 30 min for acquisition. False colour maps were generated using multi-variate curve resolution (MCR). A single data matrix, comprising all the spectra collected across the entire dissolution experiment (8092 spectra), was produced in order to probe changes as a function of both xy-position and time. Numerical codes for statistical analyses were written in the 'R' language, which is open-source and freely available [29]. Data were scaled prior to analysis and plotting using variance scaling and mean centering standard methods, as per standard practice [20] to reduce the effect of variability in Raman scattering efficiency. For multivariate curve resolution analysis, the 'ALS-MCR' module (alternating least-squares algorithm) was employed, while hierarchical agglomerative clustering is part of the standard package in R. All numerical routines along with the raw data are included in the supplementary material for information and reference.

2.5. Optical imaging

Photographic images of the compact during the dissolution were taken at regular time intervals using a CoolSNAP-Pro CF camera (Media Cybernetics) equipped with a Nikon AF Micro NIKKOR 60 mm lens. The same experimental setup described in the previous section was used, with the flow cell placed under the camera instead of the Raman microscope.

3. Results and discussion

3.1. Optical imaging

Before commencing a full discussion of the RDDR and Raman data, it is important to observe the optical images taken through the dissolution experiment for the 5% and 50% drug-loaded compacts (Fig. 1a and b). Prior to the dissolution test, both formulations appear similar, being yellowish compacts. It is important to notice the different experimental time-scales used for the two formulations. The 5% extrudate dissolution experiment was carried out for 80 min after which time the images show that the compact is completely dissolved. For the 50% drug-

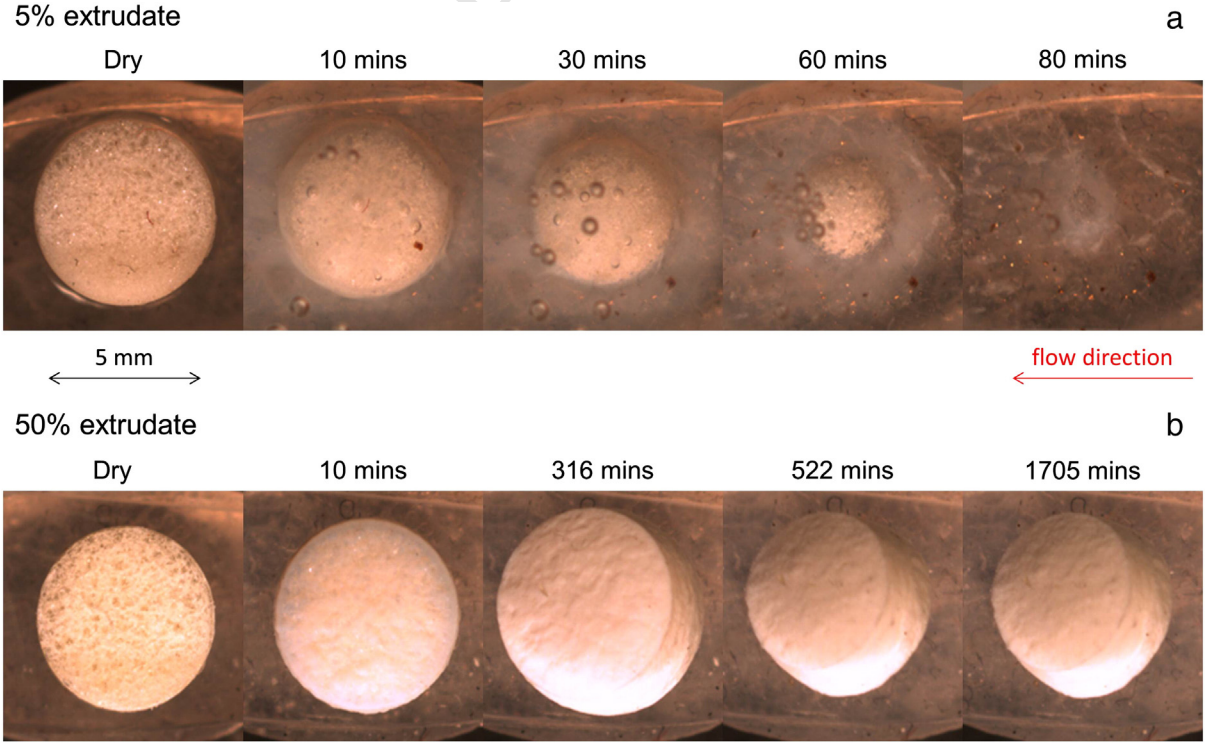

Q2 **Fig. 1.** Optical images taken through the dissolution experiment of the 5% extrudate (a) and 50% extrudate (b) compacts.

loaded formulation, time-scale was significantly longer. In total, the compact was observed in the flow cell for 1705 min, remaining intact even after the end of this period. An in depth observation of the images from the 50% extrudate shows that the compact swells and increases in size during the first 316 min, then slightly reduces and remains intact until the end of the experiment. This suggests that the initial hydration leads to swelling of the compact rather than to dissolution/erosion, due to the high content of poorly soluble felodipine in the extrudate (images until 316 min). This behaviour was previously described by Langham et al [8]. In Fig. 7 of their paper, they reported MRI sequences showing that the 50% felodipine-loaded spray-dried material swells as a result of water ingress from the dissolution medium. The visual observation of the optical images relative to the 50% extrudate is confirmed by the kinetic trend generated by counting the number of pixels of the compact during the dissolution test (Figure S3). The trend is characterised by an increase in pixel number until 316 min, which corresponds to the observed increase in the compact size. Following this, the number of pixels decreases with the rate of decrease falling to near-zero between 1093 and 1705 min, confirming that the size of the compact reduces after an initial swelling. The reduction of the compact size after an initial swelling was not previously seen in the MRI images reported by Langham et al [8]. This change in behaviour may be related to the different conditions during preparation *via* hot melt extrusion compared to spray drying (*e.g.* high temperatures, absence of solvents) which may affect the final physico-chemical properties of amorphous solid dispersions and thus their performance in aqueous media.

3.2. Rotating disk dissolution rate (RDDR)

The intrinsic dissolution rate (IDR) test has been widely used in biopharmaceutics for measuring the dissolution rate of pure active ingredients [30,31]. It is an important biopharmaceutics screening tool, and requires far less material than a traditional dissolution test. IDR measurements yield a dissolution rate normalised to the exposed surface area of the material. Formally, IDR applies only to pure drug substances [12]. Here we extend the IDR concept to formulations. By analogy with disk IDR, we define a 'rotating disc dissolution rate' RDDR. By simply coupling an IDR apparatus to a HPLC system, the partial RDDR of both the pure drug substance and the excipients (in the present case copovidone) can be measured and compared for different formulations. The partial RDDR for the drug and polymer in the different formulations are shown below to provide valuable information on the mechanism of drug release.

The dissolution rate values for the 5% and 50% drug-loaded formulations are summarised in Table 1. The dissolution profiles can be inspected in Figure S4 of the supplementary information. Partial RDDR was calculated using the first 20 minute time period, where the trend is relatively linear, in accordance with USP procedures [12]. Looking at the formulation with 5% drug loading, the partial RDDR value for felodipine is 0.17 mg/min/cm^2, while partial RDDR for copovidone is 3.10 mg/min/cm^2. The intrinsic dissolution rate value of pure crystalline felodipine has been previously found to be 0.00064 mg/min/cm^2 in pH 6.5 FaSSIF medium, so in comparison the 5% extrudate exhibits approximately a 265 fold increase in dissolution rate [32]. The significant improvement in dissolution is concurrent with literature on felodipine amorphous solid dispersions [27,33]. The dissolution rate of the polymer allows to readily calculate an index of performance of the formulation which essentially shows how the two components of the amorphous solid dispersion behave during the dissolution process. The equation to calculate the index of performance is reported in Table 1. The index of performance for the low drug-loaded extrudate results in a value of 1, indicating that felodipine and copovidone have the same dissolution trend and thus they effectively dissolve as single entity, the molecular dispersion of felodipine in copovidone. Given the very low solubility of felodipine, the release of the 5% extrudate is clearly dependent on the high water solubility of the polymer.

Turning now to the formulation with high drug loading, it is immediately evident that both felodipine and copovidone have partial RDDR values significantly lower when compared to those calculated for the 5% extrudate (Table 1). The index of performance is also very low (0.07), indicating that the dissolution rates of felodipine and copovidone are in this case very different, suggesting that the two components of the formulation are not behaving as a single entity but as two separate components. Compared to the IDR value of pure extruded copovidone (5.20 mg/min/cm^2 in pH 6.8 blank FaSSIF medium, Figure S4), copovidone present in the 50% extrudate shows approximately a 21 fold decrease in dissolution rate. RDDR data suggest that the drug release is felodipine-dependent, where low solubility in water and high hydrophobicity of the drug contribute to decrease the wettability and to slow the water uptake in the formulation.

Summarising, the 5% drug-loaded extrudate showed polymer-dependent dissolution behaviour with felodipine dissolving simultaneously with copovidone. For the 50% extrudate, the rate of felodipine released is considerably lower than that observed for the 5% drug-loaded formulation. Although the RDDR test gives a comprehensive explanation about the dissolution trend observed for the low drug-loaded formulation, it does not clearly explain why felodipine shows a very low dissolution rate for the 50% extrudate. To obtain a better understanding of the chemical changes that occur during dissolution of the formulation, Raman spectroscopic imaging was used to interrogate the samples.

3.3. Raman spectroscopy

3.3.1. Dry raw materials spectra: visual observation

The Raman spectra of the raw materials are shown in Fig. 2a (finger print) and 2b (phonon-mode). Starting with the pure components, it is evident that the spectrum of felodipine is characterised by sharp bands and a good signal/noise ratio, whereas the spectrum of copovidone shows less-defined bands. At first approximation, the amorphous solid dispersion spectra appear as a linear combination of melt quenched felodipine (amorphous reference form) and copovidone. In the 5% extrudate spectrum, copovidone bands are predominant, while in the 50% extrudate bands related to felodipine prevail. In the latter case two slight shifts appear when comparing to the spectrum of melt quenched felodipine: the band at 1209 cm^{-1} moves to a lower wavenumber, while the band at 1497 cm^{-1} appears at higher wavenumber. These changes can be ascribed to the formation of molecular interactions between the drug and the polymer coupled with minor conformational changes, as has been previously reported for amorphous solid dispersions of felodipine and PVP [11].

Turning now to the felodipine spectra, we can see significant differences between the amorphous (melt quenched felodipine) and the crystalline (felodipine as received) solid forms. Firstly, the bands of the crystalline form appear more intense and sharper than those of the amorphous form, due to the disorganised molecular environment of the amorphous solid state. Furthermore, a detailed observation highlights that the intra-molecular vibration bands at 1213, 1492 and 1645 cm^{-1} of the amorphous form slightly shift to higher wavenumber. In the phonon-mode region, which results from inter-

Table 1
Partial RDDR values of felodipine and copovidone for the 5% and 50% extrudate formulations. The index of performance was obtained dividing the partial RDDR value of felodipine by the total RDDR value of formulation (felodipine plus copovidone) and then normalising by the felodipine mass fraction.

RDDR (mg/min/cm^2)					
	Time	Felodipine	Copovidone	Total	Index of performance[a]
5% extrudate	<20 min	0.17 (±0.02)	3.10 (±0.43)	3.26	1.0
50% extrudate	<20 min	0.01 (±0.01)	0.25 (±0.01)	0.26	0.07

[a] Index of performance = (Partial RDDR felodipine / Total RDDR) / drug mass fraction.

Please cite this article as: F. Tres, et al., Real time Raman imaging to understand dissolution performance of amorphous solid dispersions, J. Control. Release (2014), http://dx.doi.org/10.1016/j.jconrel.2014.05.061

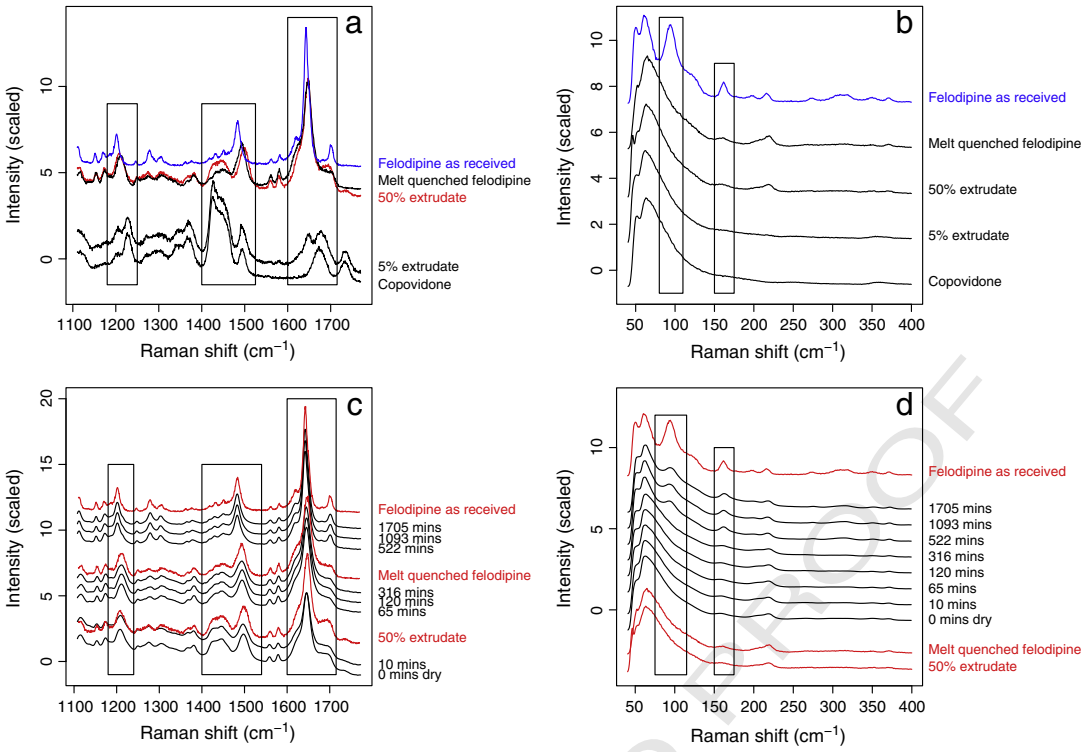

Fig. 2. Finger print (a) and phonon-mode (b) regions of raw materials spectra and finger print (c) and phonon-mode (d) regions of the averaged spectra relative to the dissolution of the 50% extrudate compact, with reference spectra in red. Y-Axis offsets were employed for presentational purposes and differ between panels. (For interpretation of the references to colour in this figure, the reader is referred to the web version of this article.)

molecular vibration, the two felodipine solid forms have different spectra. The amorphous form spectrum is characterised by broad bands and a continuous distribution of inter-molecular vibrations. In the crystalline form, sharp bands are present at 94 and 168 cm^{-1}, due to the quantised nature of the inter-molecular vibrations in the crystalline material. Thus, as reported in literature, [18,19] the phonon-mode region represents an area of the Raman spectrum where it is possible to rapidly distinguish between different solid forms.

3.3.2. Dissolution experiments

3.3.2.1. Averaged spectra: visual observation. Raman averaged spectra for the 5% extrudate dissolution are presented in Figure S5. Examination of the data does not reveal significant changes in the spectra across the entire period covered by these data (0–70 min), beyond a reduction in spectral intensity as the compact dissolves (as seen in the optical images Fig. 1a). The ratio between the band of felodipine at 1650 cm^{-1} and that of copovidone at 1426 cm^{-1} is preserved throughout the whole dissolution process. The Raman data essentially show that felodipine and copovidone dissolve as a single entity rather than as two separate components. This is in accordance with the RDDR data, which illustrated that felodipine and copovidone dissolve with the same rate. Therefore, it seems reasonable to suggest that the dissolution occurs from the molecular dispersion, with the overall behaviour being dependent on the highly-soluble polymer.

Raman data of the 50% extrudate dissolution are shown in Fig. 2c (finger print region) and d (phonon-mode region). Raman data show that the spectrum does not change after 10 min (Fig. 2c, 10 min). Bands relative to felodipine (1497 unit cm^{-1}) and copovidone (1426 cm^{-1}) preserve the same ratio as in the spectrum of the compact 'Dry'. Proceeding with the analysis, after 65 min the intensity of copovidone band at 1426 cm^{-1} appears to decrease in relation to that of felodipine at 1497 cm^{-1}. A comparison with the '50% extrudate' reference spectrum reveals that the band at 1209 cm^{-1} moves to slightly higher wavenumber and that at 1497 cm^{-1} shifts to lower wavenumber. Figure S6 presents 'difference spectra' obtained by subtracting each averaged spectrum corresponding to each time point from the averaged spectrum of the compact 'Dry', which was used in this case as reference spectrum. 'Difference spectra' between 65 and 316 min are characterised by negative bands at 1213 and 1492 cm^{-1} which correspond to the observed shifts in Fig. 2c. These spectral shifts, which were previously denoted in the visual observation of the raw ingredients spectra (Fig. 2a), unambiguously indicate a strong correlation with the melt quenched (amorphous) felodipine spectrum. It is likely that the faster dissolution of copovidone with respect to felodipine from the drug:polymer dispersion leads to a build-up of felodipine-rich amorphous material on the surface of the compact. The second important change occurs at 522 min. It is immediately obvious that the averaged spectrum, after 522 min, corresponds to the crystalline form of felodipine. When compared to melt quenched felodipine, intra-molecular bands at 1202, 1484 and 1642 cm^{-1} shift to lower wavenumber as well as they appear more intense and sharper. These spectral changes were previously seen in Fig. 2a, revealing the formation of crystalline felodipine. In the phonon-mode region (Fig. 2d), well-defined bands appear at 94 and 168 cm^{-1} after 522 min, essentially confirming that amorphous felodipine begins to re-crystallise by this time-point.

3.3.2.2. Averaged spectra: hierarchical agglomerative clustering (HAC). In this section we describe the use of an objective statistical analysis method to validate our subjective interpretation of the Raman data. HAC is an automated method of cluster analysis which calculates a distance, also called 'degree of dissimilarity', between datasets, [34] including Raman spectra [19]. The dendrogram obtained applying HAC to the 21 datasets is shown in Fig. 3. It is immediately evident that the overall structure of the dendrogram is governed by two branches: spectra relative to the dissolution of the 5% extrudate with the 5% extrudate and copovidone reference spectra, and spectra relative to the dissolution of the 50% extrudate with the remaining reference spectra ('50% extrudate', 'Melt quenched felodipine' and 'Felodipine as received'). Starting with the branch of the 5% extrudate (LHS of plot), it is clear

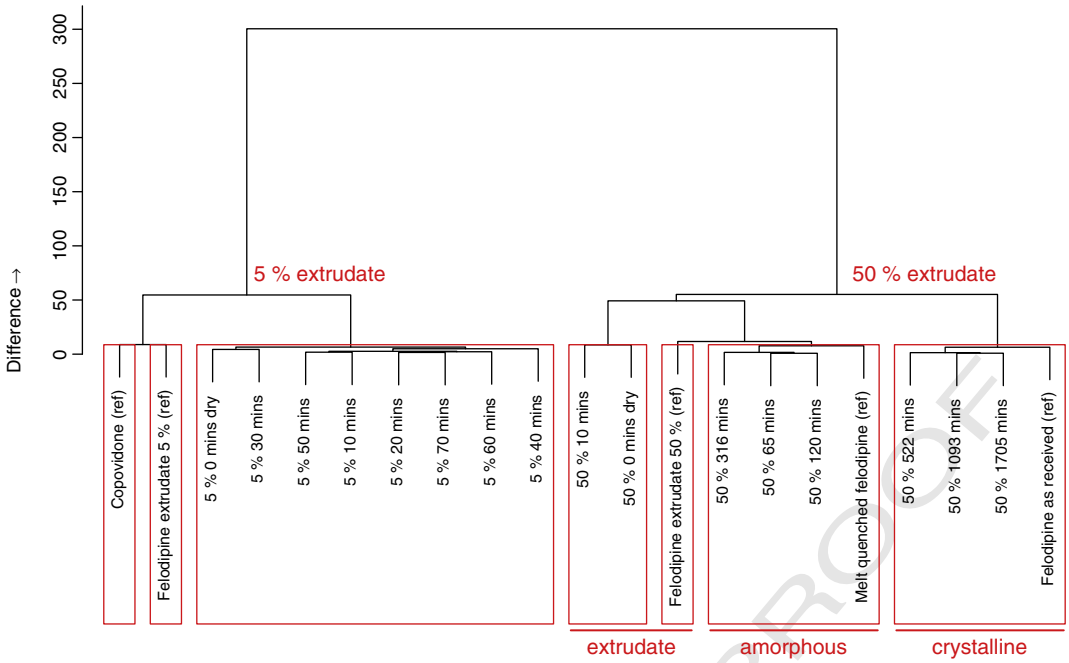

Fig. 3. Similarity dendrogram with clusters indicated by red boxes. Raw data were variance-scaled and mean-centred before performing HAC. The Euclidean distance measure was employed to define clusters. (For interpretation of the references to colour in this figure, the reader is referred to the web version of this article.)

that all the spectra relative to the dissolution can be classified by only one cluster, as they are characterised by a high degree of similarity. This trend is in a good agreement with the visual inspection of the data. As noted earlier (Figure S5), significant changes were not observed in the spectra collected during the dissolution of the 5% extrudate compact.

Turning now to the other portions of the dendrogram, that relative to the high drug-loaded formulation (RHS of plot), the presence of three main clusters is immediately apparent. The first includes '50% extrudate dry' and '50% extrudate 10 mins' spectra, which show high similarity for the 50% extrudate reference. The second cluster includes spectra collected between 65 and 361 min, with the reference spectrum of melt quenched (amorphous) felodipine. The last cluster includes spectra collected from 522 min until the end of the experiment along with the reference crystalline form of felodipine. Again, HAC confirms the visual inspection of the data, further demonstrating that two transformations occur during the dissolution of the high drug-loaded extrudate. The first involves the conversion, *via* dissolution of copovidone, of mixed extrudate into felodipine-rich amorphous material on the surface of the compact, indeed spectra collected between 65 and 361 min showed high similarity for the melt quenched reference form. The other is the re-crystallisation of the amorphous felodipine after 522 min. The first transformation clearly explains the extremely low partial RDDR values observed during the dissolution of the 50% extrudate. Copovidone cannot drive the dissolution of felodipine due to an insufficient polymer to drug ratio, resulting in formation of felodipine-rich amorphous areas on the compact surface. The disruption of the drug–polymer molecular dispersion system through loss of copovidone then induces the drug re-crystallisation.

We conclude by stating that HAC widely validated all our subjective observations of Raman data, adding to them an objective and impartial component.

3.3.2.3. Multi-variate curve resolution (MCR). We now discuss the spatially resolved images of the crystallisation event observed for felodipine present in the high drug-loaded formulation. Raman maps of the 50% extrudate compact, obtained by MCR analysis of all the spectra collected across the entire dissolution test (8092 spectra), are presented in Fig. 4. MCR results can be presented as loadings which provide the spectral phase of a specific component, and score plots that illustrate the spatial distribution of the corresponding component. Three components were required to deconvolute the mapped data. Comparison with the reference spectra unambiguously indicates that the first component, MCR1, can be associated with the extrudate and the second, MCR2, with the crystalline form of felodipine. The excellent peak to peak correlation between loadings and reference spectra confirms the utility of MCR as the statistical method to analyse spatial–temporal Raman data. MCR3 mostly picked up the background noise which characterises areas where no compact is present. The score plots show that the extrudate (MCR1) is homogenously distributed throughout the mapped compact surface before immersion in water. Corresponding MCR2 score plot indicated no traces of crystalline material in the mapped area of the dry compact. Then, the amount of crystalline felodipine (MCR2) rapidly increases at the expense of the extrudate (MCR1) after 316 min, and this is reflected by the re-crystallisation kinetic shown in Fig. 5. It is interesting to notice the complementarity of MCR1 and MCR2 score plots at 316 and 522 min, which denotes the coexistence of the extrudate and crystalline felodipine. Regions where the extrudate (MCR1) is present to its maximum are indicated by yellow colour, while the corresponding crystalline regions (MCR2) are characterised by blue colour, and *vice versa*. The re-crystallisation of amorphous felodipine evidently occurs at different rates in different regions of the compact surface, suggesting that the crystal growth stage follows an initial stage of heterogeneous nucleation. The nucleation/crystallisation process is likely linked with loss of copovidone from the extrudate. It is well known that the polymeric carrier in amorphous solid dispersion formulations not only has the function to improve the dissolution properties of poorly soluble drugs, but also inhibits crystal growth of the amorphous form, *via* antiplasticisation effect or hydrogen-bonding interactions between drug and polymer [25]. It is therefore likely that loss of copovidone during the first 316 min, previously observed in the averaged Raman spectra (Fig. 2c), promotes heterogeneous nucleation followed by crystallisation of felodipine-rich amorphous material in the compact surface.

At the end of the experiment, after 1705 min, the residue of the compact was recovered and analysed using Raman and XRPD. MCR

Please cite this article as: F. Tres, et al., Real time Raman imaging to understand dissolution performance of amorphous solid dispersions, J. Control. Release (2014), http://dx.doi.org/10.1016/j.jconrel.2014.05.061

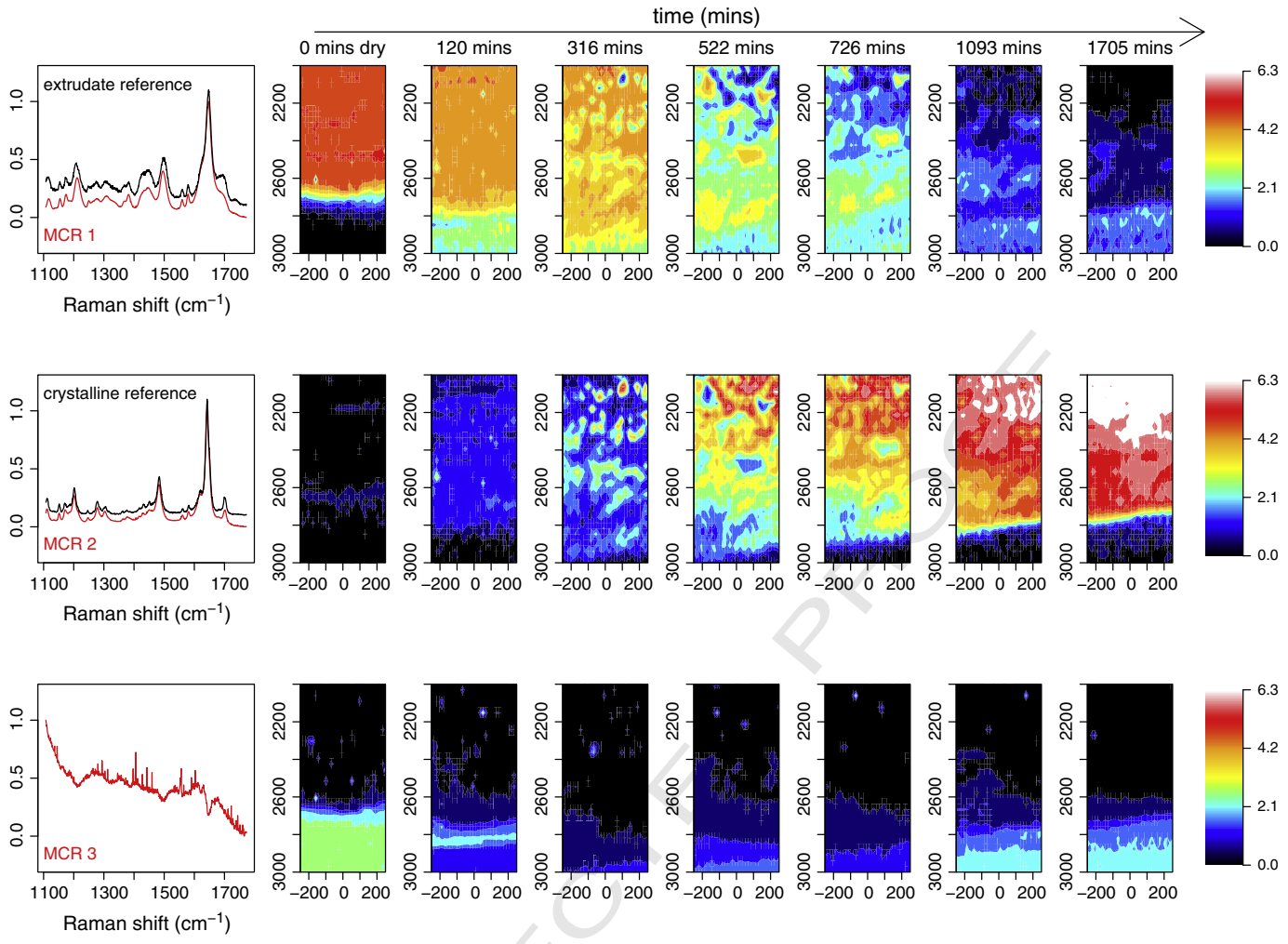

Fig. 4. Raman maps of the 50% extrudate compact as function of time, generated by MCR analysis.

maps of the core (after breaking the compact into two parts) and surface are presented in Figure S7. Two components were required in this case to deconvolute the data, with the first component (MCR1) corresponding to amorphous felodipine and the second (MCR2) corresponding to crystalline felodipine. The score plots show that felodipine is predominantly amorphous in the core, whereas in the surface is completely crystalline. Raman data suggest that the crystallisation begins from the compact surface exposed to water and propagates towards the core, where only a little amount of crystalline drug was found. The XRPD pattern of the compact after grinding it into powder can be seen in the supplementary material (Figure S1). The pattern appears as a combination of sharp bands, typical of the crystalline materials, and a broad halo which characterises the amorphous materials. XRPD therefore indicates that felodipine sampled from the entire compact after the dissolution experiment is a mixture of crystalline and amorphous. This is in full agreement with Raman results, which indicated a crystalline outer section and an amorphous inner section of the compact.

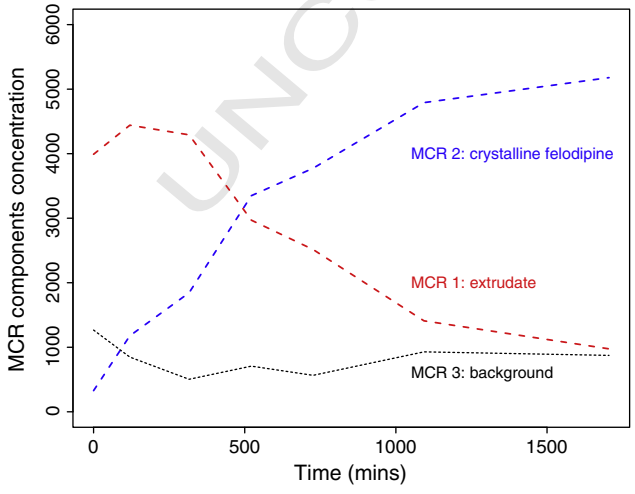

Fig. 5. Crystallisation kinetic generated by plotting the MCR component concentration in each map as function of time.

4. Conclusions

We have demonstrated that Raman imaging offers an appropriate method to investigate in real time the dissolution process and provides additional spatial information regarding the dissolution mechanisms that underpin amorphous solid dispersions, when compared to USP dissolution testing and classical Raman spectroscopy. We have successfully employed a RDDR method which allows us to track the dissolution profiles of both drug and polymer simultaneously and ultimately to measure the dissolution performance in multi-component systems. We have widely consolidated the previous findings described in Langham et al. work, [8] by generating spatially-resolved MCR Raman maps of the re-crystallisation of felodipine present in the 50% extrudate formulation. MCR Raman maps showed that amorphous felodipine

Please cite this article as: F. Tres, et al., Real time Raman imaging to understand dissolution performance of amorphous solid dispersions, J. Control. Release (2014), http://dx.doi.org/10.1016/j.jconrel.2014.05.061

crystallises at different rates in different regions of the compact surface, indicating that crystallisation follows an initial stage of heterogeneous nucleation. The re-crystallisation of felodipine leads to large variations in the Raman spectrum and thus it is readily detectable. In particular in the phonon-mode region, the spectrum of the crystalline form is characterised by clear and sharp bands, while that of the amorphous form by a broad halo. The nucleation/crystallisation process proceeds from the surface towards the core and is likely linked to loss of copovidone from the extrudate. For the 5% drug-loaded extrudate, Raman spectroscopy did not show any significant changes in the spectra collected during the course of the dissolution test. This demonstrates that felodipine and copovidone dissolve as a single entity, in accordance with the RDDR data.

5. Acknowledgements

Q4 We thank AstraZeneca and EPSRC for funding through grant EP/I01375X/1 (*via* the joint Centre for Doctoral Training in Targeted Therapeutics and Formulation Sciences). We would like to thank Richard Hart, Caroline Roger and Zoe Langham (AstraZeneca) for their helpful suggestions on the work leading to these results. We thank Jamie Patient (University of Nottingham) for his contribution to the early stages of this work. The Nottingham Nanotechnology and Nanoscience Centre is gratefully acknowledged for the access to the Raman microscope.

Appendix A. Supplementary data

Supplementary data to this article can be found online at http://dx.doi.org/10.1016/j.jconrel.2014.05.061.

References

[1] N.J. Babu, A. Nangia, Solubility advantage of amorphous drugs and pharmaceutical cocrystals, Cryst. Growth Des. 11 (7) (2011) 2662–2679.
[2] C. Leuner, J. Dressman, Improving drug solubility for oral delivery using solid dispersions, Eur. J. Pharm. Biopharm. 50 (1) (2000) 47–60.
[3] A.T.M. Serajuddin, Solid dispersion of poorly water-soluble drugs: early promises, subsequent problems, and recent breakthroughs, J. Pharm. Sci. 88 (10) (1999) 1058–1066.
[4] A. Newman, G. Knipp, G. Zografi, Assessing the performance of amorphous solid dispersions, J. Pharm. Sci. 101 (4) (2012) 1355–1377.
[5] B.C. Hancock, G. Zografi, Characteristics and significance of the amorphous state in pharmaceutical systems, J. Pharm. Sci. 86 (1) (1997) 1–12.
[6] B.C. Hancock, M. Parks, What is the true solubility advantage for amorphous pharmaceuticals? Pharm. Res. 17 (4) (2000) 397–404.
[7] D.Q.M. Craig, The mechanisms of drug release from solid dispersions in water-soluble polymers, Int. J. Pharm. 231 (2) (2002) 131–144.
[8] Z.A. Langham, J. Booth, L.P. Hughes, G.K. Reynolds, S.A.C. Wren, Mechanistic insights into the dissolution of spray-dried amorphous solid dispersions, J. Pharm. Sci. 101 (8) (2012) 2798–2810.
[9] D.E. Alonzo, G.G.Z. Zhang, D. Zhou, Y. Gao, L.S. Taylor, Understanding the behavior of amorphous pharmaceutical systems during dissolution, Pharm. Res. 27 (4) (2010) 608–618.
[10] I. Tho, B. Liepold, J. Rosenberg, M. Maegerlein, M. Brandl, G. Fricker, Formation of nano/micro-dispersions with improved dissolution properties upon dispersion of ritonavir melt extrudate in aqueous media, Eur. J. Pharm. Sci. 40 (1) (2010) 25–32.
[11] E. Karavas, G. Ktistis, A. Xenakis, E. Georgarakis, Effect of hydrogen bonding interactions on the release mechanism of felodipine from nanodispersions with polyvinylpyrrolidone, Eur. J. Pharm. Biopharm. 63 (2) (2006) 103–114.
[12] United States Pharmacopoeia 31 and National Formulary 26, The United States Pharmacopeial Convention, Inc., Rockville, Md, 2008.
[13] S.G. Kazarian, J. van der Weerd, Simultaneous FTIR spectroscopic imaging and visible photography to monitor tablet dissolution and drug release, Pharm. Res. 25 (4) (2008) 853–860.
[14] P.S. Wray, G.S. Clarke, S.G. Kazarian, Dissolution of tablet-in-tablet formulations studied with ATR-FTIR spectroscopic imaging, Eur. J. Pharm. Sci. 48 (4–5) (2013) 748–757.
[15] P. Avalle, S.R. Pygall, J. Pritchard, A. Jastrzemska, Interrogating erosion-based drug liberation phenomena from hydrophilic matrices using near infrared (NIR) spectroscopy, Eur. J. Pharm. Sci. 48 (1–2) (2013) 72–79.
[16] W. Li, A. Woldu, L. Araba, D. Winstead, Determination of water penetration and drug concentration profiles in HPMC-based matrix tablets by near infrared chemical imaging, J. Pharm. Sci. 99 (7) (2010) 3081–3088.
[17] Y.Y. Chen, L.P. Hughes, L.F. Gladden, M.D. Mantle, Quantitative ultra-fast MRI of HPMC swelling and dissolution, J. Pharm. Sci. 99 (8) (2010) 3462–3472.
[18] S. Al-Dulaimi, A. Aina, J.C. Burley, Rapid polymorph screening on milligram quantities of pharmaceutical material using phonon-mode Raman spectroscopy, CrystEngComm 12 (4) (2010) 1038–1040.
[19] A. Alkhalil, J. Babu Nanubolu, J.C. Burley, Analysis of phase transitions in molecular solids: quantitative assessment of phonon-mode vs intra-molecular spectral data, RSC Adv. 2 (1) (2012) 209–216.
[20] S. Šašić, Pharmaceutical Applications of Raman Spectroscopy, Wiley-Interscience, Hoboken, New Jersey, 2007.
[21] E. Karavas, E. Georgarakis, M.P. Sigalas, K. Avgoustakis, D. Bikiaris, Investigation of the release mechanism of a sparingly water-soluble drug from solid dispersions in hydrophilic carriers based on physical state of drug, particle size distribution and drug–polymer interactions, Eur. J. Pharm. Biopharm. 66 (3) (2007) 334–347.
[22] V. Bühler, Kollidon® Polyvinylpyrrolidone excipients for the pharmaceutical industry, 9th edition BASF, Ludwigshafen, Germany, 2008.
[23] A.C.F. Rumondor, I. Ivanisevic, S. Bates, D.E. Alonzo, L.S. Taylor, Evaluation of drug–polymer miscibility in amorphous solid dispersion systems, Pharm. Res. 26 (11) (2009) 2523–2534.
[24] P.J. Marsac, H. Konno, A.C.F. Rumondor, L.S. Taylor, Recrystallization of nifedipine and felodipine from amorphous molecular level solid dispersions containing poly (vinylpyrrolidone) and sorbed water, Pharm. Res. 25 (3) (2008) 647–656.
[25] L.S. Taylor, G. Zografi, Spectroscopic characterization of interactions between PVP and indomethacin in amorphous molecular dispersions, Pharm. Res. 14 (12) (1997) 1691–1698.
[26] A.L. Sarode, P. Wang, S. Obara, D.R. Worthen, Supersaturation, nucleation, and crystal growth during single- and biphasic dissolution of amorphous solid dispersions: polymer effects and implications for oral bioavailability enhancement of poorly water soluble drugs, Eur. J. Pharm. Biopharm. 86 (3) (2014) 351–360.
[27] Y. Song, L. Wang, P. Yang, R.M. Wenslow, B. Tan, H. Zhang, Z. Deng, Physicochemical characterization of felodipine–kollidon VA64 amorphous solid dispersions prepared by hot-melt extrusion, J. Pharm. Sci. 102 (6) (2013) 1915–1923.
[28] European Pharmacopoeia, Directorate for the Quality of Medicines and Healthcare Q6 of the Council of Europe, 6th edition, 2008. (Strasbourg, France).
[29] R.D.C. Team, R: A Language and Environment for Statistical Computing, R Foundation for Statistical Computing, Vienna, Austria, 2011. Q7
[30] L.X. Yu, A.S. Carlin, G.L. Amidon, A.S. Hussain, Feasibility studies of utilizing disk intrinsic dissolution rate to classify drugs, Int. J. Pharm. 270 (1–2) (2004) 221–227.
[31] P. Zakeri-Milani, M. Barzegar-Jalali, M. Azimi, H. Valizadeh, Biopharmaceutical classification of drugs using intrinsic dissolution rate (IDR) and rat intestinal permeability, Eur. J. Pharm. Biopharm. 73 (1) (2009) 102–106.
[32] J.H. Fagerberg, O. Tsinman, N. Sun, K. Tsinman, A. Avdeef, C.A.S. Bergström, Dissolution rate and apparent solubility of poorly soluble drugs in biorelevant dissolution media, Mol. Pharm. 7 (5) (2010) 1419–1430.
[33] E. Karavas, M. Georgarakis, A. Docoslis, D. Bikiaris, Combining SEM, TEM, and micro-Raman techniques to differentiate between the amorphous molecular level dispersions and nanodispersions of a poorly water-soluble drug within a polymer matrix, Int. J. Pharm. 340 (1–2) (2007) 76–83.
[34] F. Murtagh, A survey of recent advances in hierarchical clustering algorithms, Comput. J. 26 (4) (1983) 354–359.